

**ORGANIC POLLUTANT DEGRADATION AND HYDROGEN
PRODUCTION USING SrTiO₃ PHOTOCATALYSTS**

Tarawipa Puangpetch

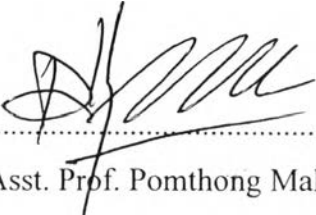
A Dissertation Submitted in Partial Fulfilment of the Requirements
for the Degree of Doctor of Philosophy
The Petroleum and Petrochemical College, Chulalongkorn University
in Academic Partnership with
The University of Michigan, The University of Oklahoma,
and Case Western Reserve University

2011


I 28375543

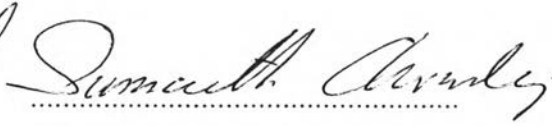
Thesis Title: Organic Pollutant Degradation and Hydrogen Production
Using SrTiO₃ Photocatalysts
By: Tarawipa Puangpetch
Program: Petrochemical Technology
Thesis Advisors: Prof. Sumaeth Chavadej
Prof. Susumu Yoshikawa
Asst. Prof. Thammanoon Sreethawong

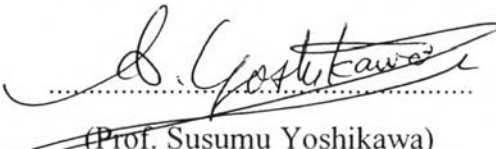
Accepted by the Petroleum and Petrochemical College, Chulalongkorn University, in partial fulfilment of the requirements for the Degree of Doctor of Philosophy.

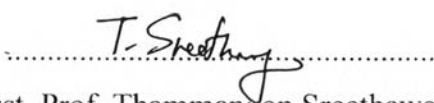

..... College Dean
(Asst. Prof. Pomthong Malakul)

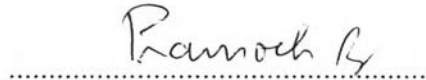
Thesis Committee:

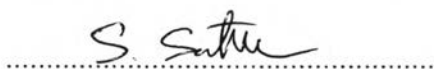

.....
(Assoc. Prof. Sujitra Wongkasemjit)


.....
(Prof. Sumaeth Chavadej)


.....
(Prof. Susumu Yoshikawa)


.....
(Asst. Prof. Thammanoon Sreethawong)


.....
(Assoc. Prof. Pramoch Rangsunvigit)


.....
(Dr. Singto Sakulkaemaruechai)

ABSTRACT

4791004063: Petrochemical Technology Program
Tarawipa Puangpetch: Organic Pollutant Degradation and Hydrogen
Production Using SrTiO₃ Photocatalysts
Thesis Advisors: Prof. Sumaeth Chavadej, Prof. Susumu Yoshikawa,
and Asst. Prof. Thammanoon Sreethawong, 160 pp.
Keywords: SrTiO₃/ Mesoporous Assembly/ Metal Loading/ Photocatalyst/
Pollutant Degradation/ Water Splitting/ Hydrogen Production

Pristine and metal-loaded mesoporous-assembled SrTiO₃ nanocrystal photocatalysts were successfully synthesized via the single-step sol-gel method with the aid of a structure-directing surfactant. The synthesis method provided the mesoporous-assembled SrTiO₃ nanocrystal photocatalysts with high purity, crystallinity, and homogeneity, as well as showed high reliability in photocatalyst reproduction. The synthesized photocatalysts were investigated their photocatalytic activity in both degradation of model organic pollutants and water splitting for hydrogen production with various hole scavengers. The results pointed out that the photocatalyst structure, in the form of a mesoporous assembly of SrTiO₃ nanocrystals, was found to be responsible for the enhancement of the photocatalytic activity of the SrTiO₃ photocatalysts. Some metals co-catalyst loading was found to enhance the photocatalytic hydrogen production activity of the mesoporous-assembled SrTiO₃-based photocatalyst. The enhancement in the photocatalytic hydrogen production activity depended on the electrochemical properties of the loaded metal type and the loading value. The 1 wt.% Au-loaded mesoporous-assembled SrTiO₃ photocatalyst was found to be the most effective photocatalyst for the hydrogen production from the photocatalytic water splitting.

บทคัดย่อ

ทรวินา พวงเพชร : การสลายสารมลพิษอินทรีย์และการผลิตก๊าซไฮโดรเจนด้วยตัวเร่งปฏิกิริยาแบบใช้แสงร่วมสตรอนเทียมไททาเนียมไดรอกไซด์ (Organic Pollutant Degradation and Hydrogen Production Using SrTiO₃ Photocatalysts) อ. ที่ปรึกษา: ศ. ดร. สุเมธ ชวเดช ศ. ดร. ชุชมุ โขชิกาวา และ ผศ. ดร. ธรรมบุญ ศรีทะวงศ์ 160 หน้า

ตัวเร่งปฏิกิริยาแบบใช้แสงร่วมสตรอนเทียมไททาเนียมไดรอกไซด์ที่มีโครงสร้างรูพรุนในระดับเมโซพอร์จากการเกาะตัวกันของผลึกระดับนาโน (mesoporous-assembled SrTiO₃ nanocrystal photocatalysts) ทั้งที่ใส่และไม่ใส่โลหะตัวเร่งปฏิกิริยาร่วม สามารถสังเคราะห์ด้วยวิธีโซล-เจล แบบใช้สารลดแรงตึงผิวช่วยในการกำหนดโครงสร้างรูพรุน โลหะตัวเร่งปฏิกิริยาร่วมจะถูกใส่ในขั้นตอนเดียวกับการสังเคราะห์ตัวเร่งปฏิกิริยาสตรอนเทียมไททาเนียมไดรอกไซด์ (single-step sol-gel method with the aid of a structure-directing surfactant) การสังเคราะห์ด้วยวิธีการนี้จะได้ตัวเร่งปฏิกิริยาที่มีค่าความบริสุทธิ์ ความเป็นผลึก และความสม่ำเสมอของเนื้อสาร อยู่ในระดับสูง รวมทั้งให้ความแน่นอนในการสังเคราะห์ซ้ำ ความสามารถในการช่วยเร่งปฏิกิริยาของตัวเร่งปฏิกิริยาที่สังเคราะห์ขึ้นถูกทดสอบด้วยปฏิกิริยาการสลายสารมลพิษอินทรีย์ตัวอย่าง และปฏิกิริยาการแตกตัวของน้ำเพื่อการผลิตก๊าซไฮโดรเจน โดยใช้ตัวเก็บโฮล (hole scavenger) หลายชนิด ผลการทดสอบบ่งชี้ว่า โครงสร้างแบบรูพรุนในระดับเมโซพอร์จากการเกาะตัวกันของผลึกระดับนาโน สามารถช่วยเพิ่มความสามารถในการช่วยเร่งปฏิกิริยาของตัวเร่งปฏิกิริยาแบบใช้แสงร่วมสตรอนเทียมไททาเนียมไดรอกไซด์สำหรับทั้งสองปฏิกิริยาที่ทดสอบ โลหะตัวเร่งปฏิกิริยาร่วมบางชนิดสามารถช่วยเพิ่มความสามารถในการช่วยเร่งปฏิกิริยาของตัวเร่งปฏิกิริยาแบบใช้แสงร่วมสตรอนเทียมไททาเนียมไดรอกไซด์สำหรับปฏิกิริยาการแตกตัวของน้ำเพื่อการผลิตก๊าซไฮโดรเจน ความสามารถในการช่วยเพิ่มความสามารถในการช่วยเร่งปฏิกิริยาขึ้นกับคุณสมบัติทางไฟฟ้าเคมีของโลหะตัวเร่งปฏิกิริยาร่วม และปริมาณการใส่โลหะตัวเร่งปฏิกิริยาร่วมลงในตัวเร่งปฏิกิริยาแบบใช้แสงร่วมสตรอนเทียมไททาเนียมไดรอกไซด์ ตัวเร่งปฏิกิริยาแบบใช้แสงร่วมสตรอนเทียมไททาเนียมไดรอกไซด์ที่มีโครงสร้างรูพรุนในระดับเมโซพอร์จากการเกาะตัวกันของผลึกระดับนาโนที่ใส่โลหะทอง 1 เปอร์เซ็นต์โดยน้ำหนัก เป็นโลหะตัวเร่งปฏิกิริยาร่วม เป็นตัวเร่งปฏิกิริยาที่มีประสิทธิภาพสูงสุดในการเร่งปฏิกิริยาการแตกตัวของน้ำเพื่อการผลิตก๊าซไฮโดรเจน

ACKNOWLEDGEMENTS

This thesis work is supported by a Project on Faculty Development in Shortage Area Scholarship (Thailand); Thailand Research Fund (TRF) and the Commission on Higher Education (Thailand); the Research Unit of Petrochemical and Environmental Catalysis, Chulalongkorn University (Thailand); the Sustainable Petroleum and Petrochemicals Research Unit, Center for Petroleum, Petrochemicals, and Advanced Materials, Chulalongkorn University (Thailand); and Institute of Advanced Energy, Kyoto University (Japan). This thesis work is partially funded by Postgraduate Education and Research Programs in Petroleum and Petrochemical Technology (PPT Consortium).

The author would like to express her sincere gratitude to Prof. Sumaeth Chavadej, Asst. Prof. Thammanoon Sreethawong, and Prof. Susumu Yoshikawa, her advisors, for their invaluable support, encouragement, supervision and useful suggestions throughout this research work. Their support and continuous guidance enabled the author to complete her work successfully.

She would like to express special thanks to Assoc. Prof. Sujitra Wongkasemjit, Assoc. Prof. Pramoch Rangsunvigit, and Dr. Singto Sakulkaemaruehai for kindly serving on her thesis committee and their valuable suggestions throughout this study.

Her gratitude is absolutely extended to all staffs of the Petroleum and Petrochemical College, Chulalongkorn University, for all their kind assistance and cooperation and to her friends for their unforgettable friendship and support.

Furthermore, her sincere thanks go to her husband and sons, who shared their love and experiences with her.

Finally, she really would like to express her sincere gratitude to her parents for their love, understanding, and support throughout her life.

TABLE OF CONTENTS

	PAGE
Title Page	i
Abstract (in English)	iii
Abstract (in Thai)	iv
Acknowledgements	v
Table of Contents	vi
List of Tables	xi
List of Figures	xii
CHAPTER	PAGE
I INTRODUCTION	1
1.1 Rationale and Problems	1
1.2 Objectives	3
1.3 Scope of Research Work	3
1.4 References	5
II THEORETICAL BACKGROUND AND LITERATURE REVIEWS	9
2.1 Elementary Processes in Photocatalysis Using Semiconductors	9
2.2 Photocatalytic Decomposition of Water for Hydrogen Production	12
2.2.1 Thermochemical Water Splitting With the Sulfur-Iodine Cycle (S-I Cycle)	12
2.2.2 Direct Water Splitting at High Temperatures Using a Mixed Conducting Membrane	12
2.2.3 Water Electrolysis	13
2.2.4 High Temperature Electrolysis or Steam Electrolysis	14
2.2.5 Steam Reforming	15
2.2.6 Photocatalytic Decomposition of Water	15

CHAPTER	PAGE
2.3 Chemical Addition for H ₂ Production Enhancement	19
2.3.1 Hole Scavenger Reagent to Suppress Electron-Hole Recombination	19
2.3.2 Chemical Additives to Suppress the Backward Reaction of H ₂ and O ₂	20
2.4 Photocatalyst Modification for H ₂ Production Enhancement	21
2.4.1 Ion Doping	21
2.4.1.1 Metal Ion Doping	21
2.4.1.2 Anion Doping	22
2.4.2 Metal or Co-Catalyst Loading	23
2.4.3 Dye Sensitization	25
2.4.4 Composite Semiconductor Photocatalysts	27
2.4.5 Structure and Morphology Control of Photocatalysts	29
2.5 Photocatalytic Degradation of Organic Pollutants	31
2.6 References	36
 III EXPERIMENTAL	 44
3.1 Chemicals	44
3.2 Photocatalyst Synthesis Methods	45
3.3 Characterization Techniques	46
3.4. Photocatalytic Activity Testing	49
3.4.1 The Photodegradation of Methyl Orange	49
3.4.2 The Photocatalytic Hydrogen Production	49
3.5 References	52
 IV SYNTHESIS AND PHOTOCATALYTIC ACTIVITY IN METHYL ORANGE DEGADRATION OF MESOPOROUS-ASSEMBLED SrTiO₃ NANOCRYSTALS PREPARED BY SOL-GEL METHOD WITH THE AID OF STRUCTURE-DIRECTING SURFACTANT	 53
Abstract	53

CHAPTER	PAGE
4.1 Introduction	53
4.2 Experimental	55
4.2.1 Materials	55
4.2.2 Synthesis Procedure	56
4.2.3 Characterization Techniques	56
4.2.4 Photocatalytic Activity Testing	58
4.3 Results and Discussion	59
4.3.1 Effects of Synthesis Conditions	59
4.3.2 Characterization Results	60
4.3.3 Photocatalytic Activity Results	74
4.4 Conclusions	79
4.5 Acknowledgments	79
4.6 References	80
V	
HYDROGEN PRODUCTION FROM	82
PHOTOCATALYTIC WATER SPLITTING OVER	
MESOPOROUS-ASSEMBLED SrTiO₃	
NANOCRYSTAL-BASED PHOTOCATALYSTS	
Abstract	82
5.1 Introduction	83
5.2 Experimental	84
5.2.1 Materials	84
5.2.2 Synthesis Procedure of Mesoporous-Assembled SrTiO ₃ Photocatalysts	85
5.2.3 Photocatalyst Characterization Techniques	86
5.2.4 Photocatalytic Water Splitting Experiments	87
5.3 Results and Discussion	89
5.3.1 Photocatalyst Characterization Results	89
5.3.2 Effects of Type and Concentration of Hole Scavenger	95
5.3.3 Effect of Pt Loading	98

CHAPTER	PAGE
5.3.4 Effect of MeOH Volume Fraction and Reaction Temperature	100
5.3.5 Photocatalyst Durability and Reuse	104
5.4 Conclusions	107
5.5 Acknowledgments	108
5.6 References	109
 VI HYDROGEN PRODUCTION OVER METAL-LOADED MESOPOROUS-ASSEMBLED SrTiO₃ NANOCRYSTAL PHOTOCATALYSTS: EFFECTS OF METAL TYPE AND LOADING	 112
Abstract	112
6.1 Introduction	112
6.2 Experimental	114
6.2.1 Materials	114
6.2.2 Synthesis procedure of mesoporous-assembled SrTiO ₃ photocatalysts	115
6.2.3 Photocatalyst characterization techniques	115
6.2.4 Photocatalytic hydrogen production system	116
6.3 Results and discussion	117
6.3.1 Characterization results	117
6.3.2 Effect of metal loading on hydrogen production activity of the SrTiO ₃ -based photocatalysts	123
6.3.3 Effect of photocatalyst dosage	126
6.3.4 Effect of gas phase-to-liquid phase volumetric ratio	129
6.4 Conclusions	129
6.5 Acknowledgments	130
6.6 References	131

CHAPTER	PAGE
VII HYDROGEN PRODUCTION OVER Au-LOADED MESOPOROUS-ASSEMBLED SrTiO₃ NANOCRYSTAL PHOTOCATALYST: EFFECTS OF MOLECULAR STRUCTURE AND CHEMICAL PROPERTIES OF HOLE SCAVENGERS	136
Abstract	136
7.1 Introduction	136
7.2 Experimental	138
7.2.1 Materials	133
7.2.2 Synthesis procedure of photocatalysts	139
7.2.3 Photocatalyst characterization techniques	139
7.2.4 Photocatalytic hydrogen production system	140
7.3 Results and discussion	141
7.3.1 Photocatalyst characterization results	141
7.3.2 Photocatalytic hydrogen production results	144
7.4 Conclusions	150
7.5 Acknowledgments	151
7.6 References	152
VIII CONCLUSIONS AND RECOMMENDATIONS	156
8.1 Conclusions	156
8.2 Recommendations	157
CURRICULUM VITAE	158

LIST OF TABLES

TABLE	PAGE
2.1 Results of the SrTiO ₃ -based photocatalysts for photocatalytic decomposition of water for hydrogen production	33
2.2 Results of the SrTiO ₃ -based photocatalysts for photocatalytic decomposition of various pollutants	34
4.1 Thermal decomposition behaviors obtained from the TG-DTA analysis of photocatalysts prepared by using different solvents	62
4.2 Band gap wavelength (λ_g), the band gap energy (E_g), and crystallite size of SrTiO ₃ synthesized by using different surfactants: LAHC, CTAB, and CTAC, commercial SrTiO ₃ (Wako)	69
4.3 Band gap wavelength (λ_g), the band gap energy (E_g), and crystallite size of SrTiO ₃ synthesized by using different LAHC-to-TIPT molar ratios: 0.25:1, 0.5:1, 0.75:1, and 1:1, as compared to commercial SrTiO ₃ (Wako)	72
5.1 Physical and textural properties of all investigated photocatalysts	90
6.1 Textural properties of all studied photocatalysts from XRF, XRD, UV-visible spectroscopy, and N ₂ adsorption-desorption analyses	120
7.1 Comparative results of specific H ₂ production rate from the photocatalytic water splitting over various SrTiO ₃ -based photocatalysts	149

LIST OF FIGURES

FIGURE	PAGE
2.1 Electron-hole pair generation in a photo-irradiated n-type photocatalyst	9
2.2 The plot between the Kabelka-Munk function ($F(R)$) as a function of wavelength (λ , nm) and the band gap wavelength (λ_g) estimation	10
2.3 The concept of hydrogen production from direct water splitting at high temperatures using a mixed conducting membrane	13
2.4 The Hoffman electrolysis apparatus used in electrolysis of water	14
2.5 Schematic of high temperature electrolysis	15
2.6 Band gap energy of the photocatalyst	17
2.7 Band edge positions of semiconductors as determined in photoelectrochemical experiments with respect to a normal hydrogen electrode (NHE) as reference points, and the standard redox potentials of water in acidic	17
2.8 Mechanism of dye-sensitized photocatalysis under light irradiation	26
2.9 Electron injection in composite semiconductors	27
2.10 Cubic perovskite SrTiO ₃	30
3.1 Schematic of the synthesis procedure	46
3.2 The plot between the Kabelka-Munk function ($F(R)$) as a function of wavelength (λ , nm) and the band gap wavelength (λ_g) estimation	48
3.3 The photocatalytic hydrogen production system used in this study	50

FIGURE	PAGE
4.1 TG-DTA curves of the synthesized SrTiO ₃ samples (zero gels) (LAHC as a structure-directing surfactant and a LAHC-to-TIPT molar ratio of 0.25:1) prepared by using different solvents: (a) EG, (b) EtOH, and (c) an EtOH/EG mixture (EtOH-to-EG volumetric ratio of 0.1:1)	61
4.2 XRD patterns of the synthesized SrTiO ₃ (a calcination temperature of 700°C, a heating rate of 1°C min ⁻¹ , and a TIPT-to-LAHC molar ratio of 1:0.25) prepared with different solvents: EtOH, EG, and an EtOH/EG mixture (EtOH-to-EG volumetric ratio of 0.1:1), as compared to the commercial SrTiO ₃ (Wako)	63
4.3 XRD patterns of the synthesized SrTiO ₃ (EtOH as a solvent, a calcination temperature of 700°C, a heating rate of 1°C min ⁻¹ , and a surfactant-to-TIPT molar ratio of 0.25:1) using different surfactants: LAHC, CTAB, and CTAC, as compared to the commercial SrTiO ₃ (Wako)	64
4.4 XRD patterns of the synthesized SrTiO ₃ (EtOH as a solvent, a heating rate of 1°C min ⁻¹ , and a LAHC-to-TIPT of 0.25:1) calcined at different calcination temperatures	65
4.5 N ₂ adsorption-desorption isotherms, specific surface area, and pore size distributions of (a) the commercial SrTiO ₃ (Wako), and the synthesized SrTiO ₃ (a calcination temperature of 700°C, a heating rate of 1°C min ⁻¹ , and a LAHC-to-TIPT molar ratio of 0.25:1) using different solvents: (b) EG, (c) EtOH, and (d) an EtOH/EG mixture	66

FIGURE	PAGE
4.6 N ₂ adsorption-desorption isotherms, specific surface area, and pore size distributions of (a) the commercial SrTiO ₃ (Wako), and the synthesized SrTiO ₃ (EtOH as a solvent, a calcinations temperature of 700°C, a heating rate of 1°C min ⁻¹ , and a surfactant-to-TIPT molar ratio of 0.25:1) using different surfactants: (b) LAHC, (c) CTAB, and (d) CTAC	67
4.7 The plot between $F(R)$ and λ of the SrTiO ₃ samples (EtOH as a solvent, a calcination temperature of 700°C, a heating rate of 1°C min ⁻¹ , and a surfactant-to-TIPT molar ratio of 0.25:1) synthesized with different surfactants: LAHC, CTAB, and CTAC, as compared to the commercial SrTiO ₃ (Wako)	69
4.8 (a) Pore size distribution and (b) specific surface area of the SrTiO ₃ samples prepared with different LAHC-to-TIPT molar ratios using EtOH as a solvent, 700°C calcination temperature, and 1°C min ⁻¹ heating rate	71
4.9 Plot between $F(R)$ and λ of the SrTiO ₃ samples (EtOH as a solvent, a calcination temperature of 700°C, and a heating rate of 1°C min ⁻¹) prepared with different LAHC-to-TIPT molar ratios, as compared to commercial SrTiO ₃ (Wako)	72
4.10 TEM images of (a) the commercial SrTiO ₃ (Wako), and the synthesized SrTiO ₃ (EtOH as a solvent, a heating rate of 1°C min ⁻¹ , and a LAHC-to-TIPT molar ratio of 0.25:1) calcined at different calcination temperatures: (b) 600°C, (c) 650°C, and (d) 700°C	74

FIGURE	PAGE
4.11 (a) Time course of the percentage of methyl orange degradation over the synthesized SrTiO ₃ photocatalysts and (b) the specific surface area and the pseudo-first-rate constant of the synthesized SrTiO ₃ photocatalysts, as compared to the commercial SrTiO ₃ (Wako). The synthesized SrTiO ₃ photocatalysts were prepared under the optimum conditions (EtOH as a solvent, a heating rate of 1°C min ⁻¹ , and a LAHC-to-TIPT molar ratio of 0.25:1) at different calcination temperatures	76
4.12 (a) Time course of the percentage of methyl orange degradation over the synthesized SrTiO ₃ photocatalysts and (b) the specific surface area and the pseudo-first-rate constant of the synthesized SrTiO ₃ photocatalysts, as compared to the commercial SrTiO ₃ (Wako). The synthesized SrTiO ₃ photocatalysts were prepared under the optimum conditions (EtOH as a solvent, a calcination temperature of 700°C, and a heating rate of 1°C min ⁻¹) at different LAHC-to-TIPT molar ratios	78
5.1 XRD patterns of the SrTiO ₃ photocatalysts	90
5.2 TEM images of the SrTiO ₃ photocatalysts: (a) commercial SrTiO ₃ , (b) pristine SrTiO ₃ , (c) 0.5 wt.% Pt-loaded SrTiO ₃ , and HRTEM images of the 0.5 wt.% Pt-loaded SrTiO ₃ to show (d) d spacing of SrTiO ₃ (110) and (e) d spacing of Pt ⁰ (111)	91
5.3 N ₂ adsorption-desorption isotherm and pore size distribution (inset) of (a) the pristine mesoporous-assembled SrTiO ₃ photocatalyst, (b) the 0.5 wt.% Pt-loaded SrTiO ₃ , and (c) the commercial SrTiO ₃	93

FIGURE	PAGE
5.4 Aggregated particle size distributions of the commercial SrTiO ₃ and the mesoporous-assembled SrTiO ₃ photocatalysts: pristine SrTiO ₃ and 0.5 wt.% Pt-loaded SrTiO ₃	94
5.5 Deconvoluted Pt4f XPS spectra of the 0.5 wt.% Pt-loaded SrTiO ₃ photocatalyst	94
5.6 Plot of (a) reflectance and (b) F(r) as a function of wavelength of the commercial SrTiO ₃ and the mesoporous-assembled SrTiO ₃ photocatalysts: pristine SrTiO ₃ and 0.5 wt.% Pt-loaded SrTiO ₃	95
5.7 Dependence of H ₂ production rate over the 0.5 wt.% Pt-loaded SrTiO ₃ photocatalyst under UV irradiation on type and concentration of hole scavengers (studied conditions: 5 h irradiation time, 500 ml of aqueous solution, 0.5 g of photocatalyst, reaction temperature of 15°C)	96
5.8 Effects of the reactant system, the presence of a photocatalyst, and the reaction temperature on H ₂ production (the overall rate of reaction at 5 h, 500 ml of solution, 0.5 g of 0.5 wt. % Pt-loaded SrTiO ₃ photocatalyst, and UV irradiation). Note: the units of the H ₂ production rate is $\mu\text{mol h}^{-1}$ or $\mu\text{mol h}^{-1} \text{g}_{\text{cat}}^{-1}$ in the case of no photocatalyst addition and in the case of photocatalyst addition, respectively	97
5.9 H ₂ production rate under UV and visible light irradiation as a function of Pt loading over the synthesized SrTiO ₃ (studied conditions: 5 h irradiation time, 500 ml of 50 vol.% MeOH aqueous solution, 0.5 g of photocatalyst, reaction temperatures of 45°C for UV irradiation and 30°C for visible light irradiation)	99

FIGURE	PAGE
5.10 Dependences of H ₂ production rate (a), H ₂ production enhancement by MeOH (b), and apparent activation energy (\hat{E}_a) of the photocatalytic water splitting reaction (c) on the MeOH concentration and reaction temperature (studied conditions: 5 h irradiation time, 500 ml of solution, 0.5 g of 0.5 wt.% Pt-loaded SrTiO ₃ photocatalyst, and UV irradiation)	103
5.11 Time course of (a) accumulative H ₂ production and (b) instantaneous H ₂ production rate over the 0.5 wt.% Pt-loaded SrTiO ₃ photocatalyst under UV irradiation (studied conditions: 500 ml of 50 vol.% MeOH aqueous solution, 0.5 g of photocatalyst, and a reaction temperature of 45°C)	105
5.12 Time course of H ₂ production over the fresh and spent 0.5 wt.% Pt-loaded SrTiO ₃ photocatalyst under UV irradiation (studied conditions: 500 ml of 50 vol.% MeOH aqueous solution, 0.5 g of photocatalyst, and a reaction temperature of 45°C)	106
6.1 XRD patterns of the pristine and the 0.5 wt.% metal-loaded SrTiO ₃ photocatalysts	118
6.2 Plot of the Kabelka–Munk function (F(r)) as a function of wavelength of the pristine and the 0.5 wt.% metal-loaded SrTiO ₃ photocatalysts	121
6.3 N ₂ adsorption–desorption isotherms of the pristine and the 0.5 wt.% metal-loaded SrTiO ₃ photocatalysts: (a) unloaded, (b) Au, (c) Pt, (d) Ni, (e) Ag, (f) Ce, and (g) Fe	122

FIGURE	PAGE
6.4 Dependence of H ₂ production efficiency under (a) UV light irradiation and (b) visible light irradiation on type and quantity of metal loading (system conditions: 5 h irradiation time, 500 (UV) and 200 (visible) cm ³ of a 50 vol.% MeOH aqueous solution, and photocatalyst weight of 0.5(UV) and 0.2 (visible) g)	124
6.5 Dependence of H ₂ production efficiency on (a) photocatalyst dosage (system conditions: 5 h irradiation time, 200 cm ³ of a 50 vol.% MeOH aqueous solution, photocatalyst weight of 0.1-1.5 g, 1 wt.% Au-loaded SrTiO ₃ photocatalyst, and visible light irradiation) and (b) gas phase-to-liquid phase volumetric ratio (system conditions: 5 h irradiation time, 50 vol.% MeOH aqueous solution, photocatalyst dosage of 1×10 ⁻³ g cm ⁻³ , photocatalyst weight of 0.05-0.6 g, 1 wt.% Au-loaded SrTiO ₃ photocatalyst, and UV light irradiation)	127
7.1 XRD pattern of the 1 wt.% Au-loaded mesoporous-assembled SrTiO ₃ photocatalyst	142
7.2 TEM image of the 1 wt.% Au-loaded mesoporous-assembled SrTiO ₃ photocatalyst.	142
7.3 N ₂ adsorption–desorption isotherms (a) and pore size distribution (b) of the 1 wt.% Au-loaded mesoporous-assembled SrTiO ₃ photocatalyst.	143
7.4 Dependence of specific H ₂ production rate on type and concentration of the hole scavengers (system conditions: 5 h irradiation time, 200 cm ³ of aqueous hole scavenger solution, 0.2 g of 1 wt.% Au-loaded mesoporous-assembled SrTiO ₃ photocatalyst, and 45°C reaction temperature)	145

FIGURE**PAGE**

- 7.5 Dependence of specific H₂ production rate on initial solution pH value of the hole scavenger aqueous solution (system conditions: 5 h irradiation time, 200 cm³ of aqueous hole scavenger solution, 2.5 vol.% of hole scavenger concentration, 0.2 g of 1 wt.% Au-loaded mesoporous-assembled SrTiO₃ photocatalyst, and 45°C reaction temperature)

147